Large-scale single-crystal blue phase through holography lithography

Xiaowan Xu, Jiawei Wang, Yanjun Liu, and Dan Luo*

Department of Electrical & Electronic Engineering, Southern University of Science and Technology, Xueyuan Road 1088, Nanshan District, Shenzhen, Guangdong, 518055, China.
E-mail: luod@sustech.edu.cn

Theory of free energy of blue phase liquid crystals

The free energy is described by the Laudan de Gennes equation consist of three parts: the short-range free energy density (f_P) which describes the phase transition, the long-range free energy density (f_E) which describes the elastic distortions, the surface free energy density (f_S) which describes the surface contribution, given by:

$$F = \int d^3x(f_P + f_E) + \int d^2x(f_S) \quad , \tag{S1}$$

$$f_P = \frac{1}{2}a(T - T^*)Q_{xy}Q_{yx} + \frac{1}{3}BQ_{xy}Q_{yz}Q_{zx} + \frac{1}{4}C(Q_{xy}Q_{yx})^2 \quad , \tag{S2}$$

where a, B, and C are nematic material parameters, T is temperature and T^* is the supercooling temperature, and Q_{ij} is the tensor order parameter field of liquid crystal to characterize all the orientational degrees. The tensor order parameter is defined as,

$$Q_{ij} = S(n_i n_j - \frac{1}{3}\delta_{ij}), \tag{S3}$$

where i,j =1, 2, 3 and n_i are the x, y, z components of the local director vector; S is the scalar order parameter, where $S \le 3/2\cos^2\theta - 1/2 >$, with $\cos\theta = \boldsymbol{a}\cdot\boldsymbol{n}$, where $\boldsymbol{a}$ is the molecular orientation and < > denotes a spatial average.

$$f_E = \frac{1}{2}L_1\frac{\partial Q_{ij}\partial Q_{ij}}{\partial x_k \partial x_k} + \frac{1}{2}L_2\frac{\partial Q_{ij}\partial Q_{ik}}{\partial x_j \partial x_k} + \frac{1}{2}L_3 Q_{ij}\frac{\partial Q_{kl}\partial Q_{kl}}{\partial x_i \partial x_j} + 2q_0 L_4 \varepsilon_{ikl} Q_{ij}\frac{\partial Q_{ij}}{\partial x_k}, \tag{S4}$$

where L_i are the elastic constant of liquid crystal and are independent of the nematic degree of order, q_0 is a chiral parameter related to the pitch of the cholesteric helix p_0 by $q_0 = \frac{2\pi}{p_0}$, and ε_{ikl} is the fully antisymmetric alternating tensor equal to +1 (-1) if i,k,l is an even (odd) permutation

of 1,2,3 and zero otherwise.

For homeotropic anchoring surface, the uniform surface anchoring is typically modeled by using a Rapini-Papoular-like surface free energy density functional,

$$f_S^H = \frac{1}{2} W^H (Q_{ij} - Q_{ij}^0)^2, \tag{S5}$$

where Wuni is the uniform surface anchoring strength and Q_{ij}^0 is the surface-preferred order parameter tensor.

For planar anchoring surface, it imposes not only uniform but also degenerate surface ordering where molecules prefer to lie in a plane with no in-plane preferred direction. Such a degenerate planar surface functional was introduced by Fournier and Galatola,

$$f_S^P = W_1(\tilde{Q}_{ij} - \tilde{Q}_{ij}^{\perp})^2 + W_2(\tilde{Q}_{ij}\tilde{Q}_{ij} - 9S_0^2)^2, \tag{S6}$$

where W_1 and W_2 are two surface anchoring constants, S_0 is the surface preferred degree of order, $\tilde{Q}_{ij} = Q_{ij} + \frac{1}{3} S_0 \delta_{ij}$, and $\tilde{Q}_{ij}^{\perp} = P_{ik}\tilde{Q}_{kl}P_{lj}, P_{ij} = \delta_{ij} - v_i v_j$, P_{ij} is surface projections, v_i is surface normal.

Fig. S1
The morphology of BPI (110) lattice plane at the cutting length l_c from 0 to d)

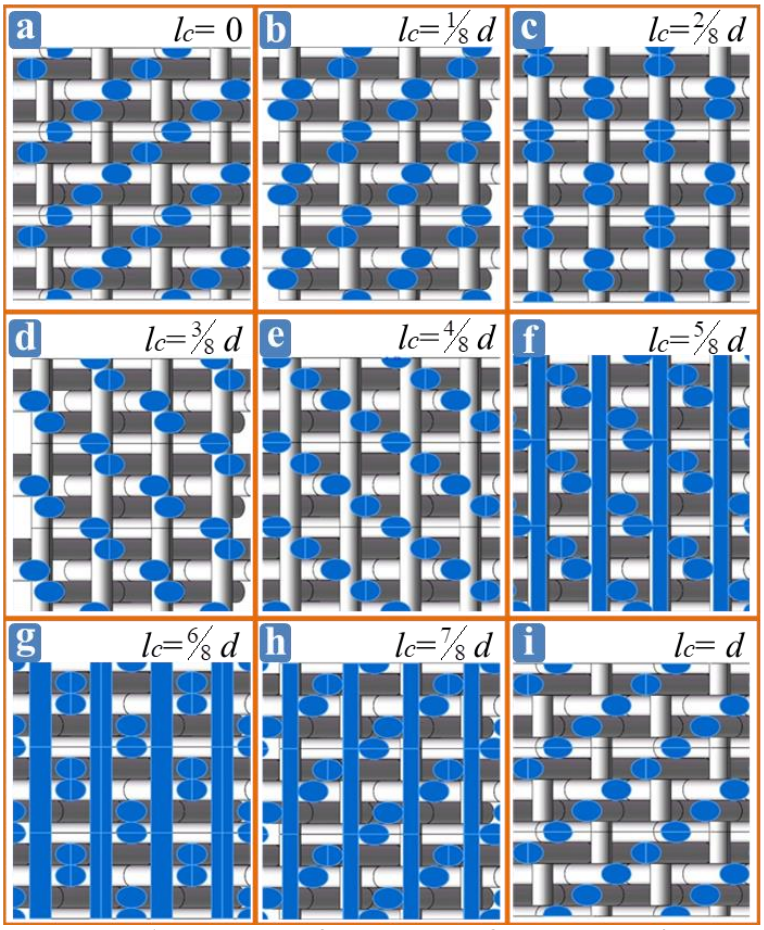

Fig. S1. (a) $l_c = 0$; (b) $l_c = \frac{1}{8}d$; (c) $l_c = \frac{2}{8}d$; (d) $l_c = \frac{3}{8}d$; (e) $l_c = \frac{4}{8}d$; (f) $l_c = \frac{5}{8}d$; (g) $l_c = \frac{6}{8}d$; (h) $l_c = \frac{7}{8}d$; (i) $l_c = d$; where d is the period of lattice plane (110), and $d = \frac{\sqrt{2}}{2}a_{BPI}$.

Fig. S2
The morphology of BPII (100) lattice plane at the cutting length l_c from 0 to d.

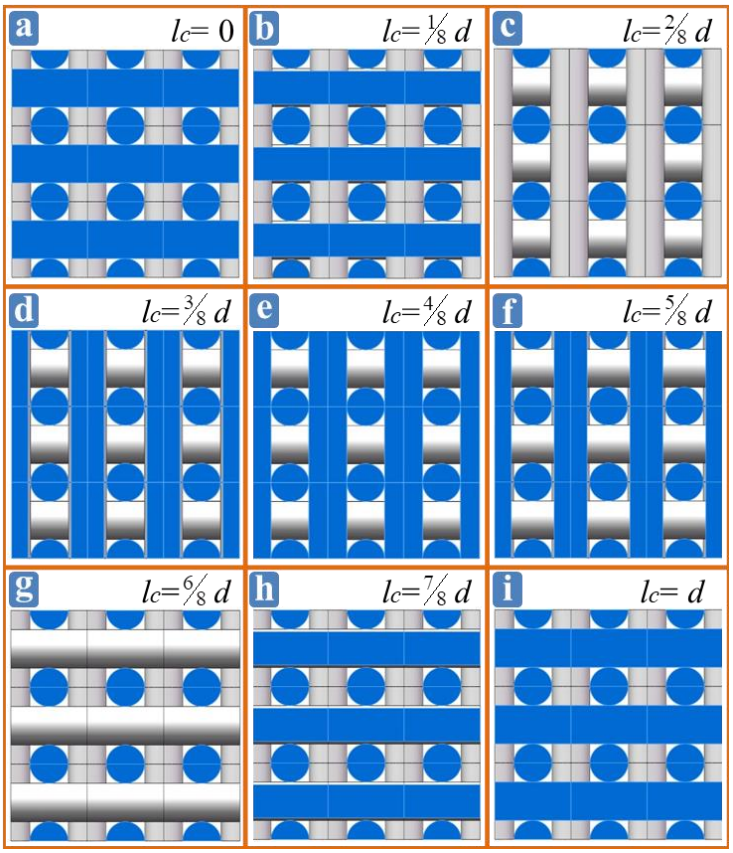

Fig. S2. (a) $l_c = 0$; (b) $l_c = \frac{1}{8}d$; (c) $l_c = \frac{2}{8}d$; (d) $l_c = \frac{3}{8}d$; (e) $l_c = \frac{4}{8}d$; (f) $l_c = \frac{5}{8}d$; (g) $l_c = \frac{6}{8}d$; (h) $l_c = \frac{7}{8}d$; (i) $l_c = d$; where d is the period of lattice plane (100), and $d = a_{BPII}$.

Fig. S3
The comparision of single crystalline BPs from polydomain and monodomain BPs in spectra and POM images.

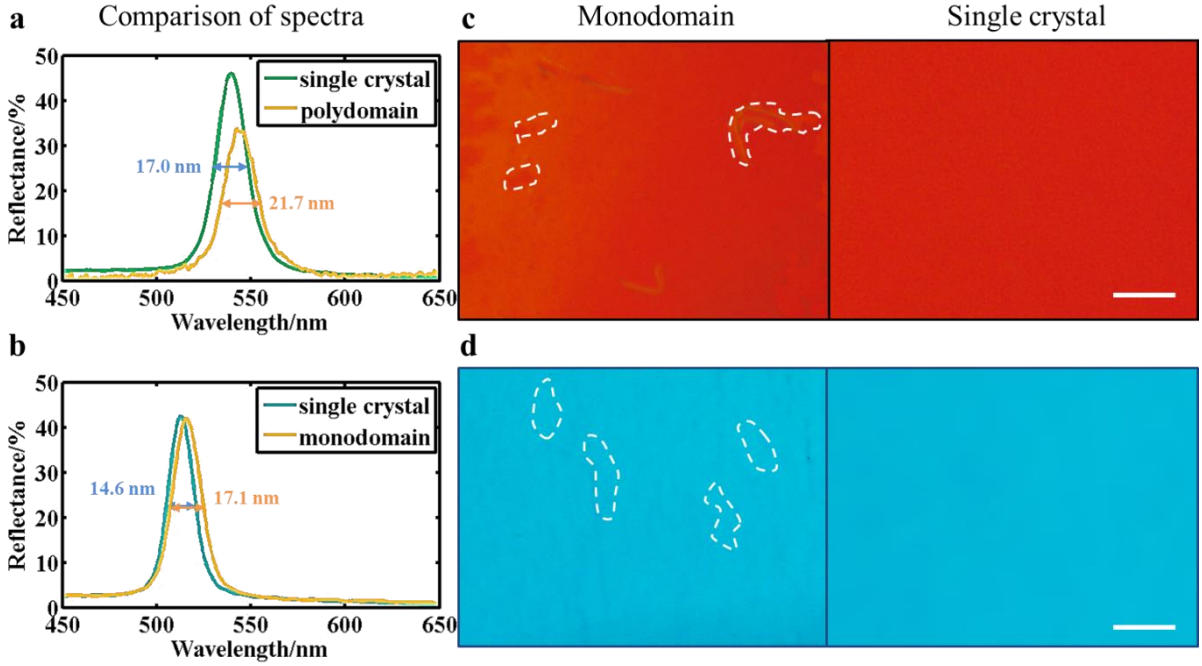

Fig. S3. (a) Comparison of reflection spectra between single-crystal and polydomain BPs. (b) Comparison of reflection spectra between single-crystal and monodomain BPs. (c) The POM images of monodomain and single-crystal BPI; the white dotted lines are the boundary of fragments in lattice structures. (d) The POM images of monodomain and single-crystal BPII. The scale bar is 100 μm.